JOURNAL OF SOLID STATE CHEMISTRY **123,** 109–114 (1996)
ARTICLE NO. 0158

Influence of Co/Fe Ratio on the Synthesis of Cobalt Containing Metal–Spinel Composites by Using Iron Disproportionation

S. Läkamp and G. Pourroy

IPCMS, Groupe des Matériaux Inorganiques, 23 Rue du Loess, 67037 Strasbourg Cedex, France

Received September 19, 1995; in revised form January 17, 1996; accepted January 18, 1996

Metal–spinel composites made up of an iron–cobalt alloy and a cobalt-doped magnetite are synthesized by using the disproportionation of $Fe(OH)_2$ and the reduction of Co(II) by Fe^0 in a concentrated and hot KOH solution. The effect of the Co/Fe ratio ($0 \leq Co/Fe \leq 1$) on the composition and the structure is described. Two KOH concentrations, 9.0 and 11.5 mol/liter, have been considered. A partial dissolution of cobalt hydroxide in KOH occurs. The metallic part always contains an iron–cobalt alloy of bcc structure. Additional diffraction lines occur, favored by high Co/Fe ratios. They are assigned to a metallic phase, either a fcc structure and an unknown structure close to the hexagonal cobalt, or a cobalt–iron alloy of hexagonal structure with $a = 7.136$ (2) Å and $c = 2.186$ (2) Å. In vacuum, the composites undergo a transformation into the wüstite phase. The temperature range of the transformation increases with a further increase of Co/Fe.

INTRODUCTION

Metal–ceramic composites are widely studied for their mechanical or magnetic properties (1, 2). A common method for preparing metal–ceramic nanocomposites is the reduction of transition metal oxides such as Al_2O_3 or SiO_2 (3, 4). For instance, Fe/Al_2O_3 or Cu/SiO_2 composites are prepared by reduction of small particles of oxides Fe_2O_3, CuO, or Cu_2O in oxides or gels and have found application in fundamental physics (5, 6). High energy ball milling of metal and oxides is another way to obtain composite materials at room temperature: for instance, mixing of Fe_2O_3, Cr_2O_3, and Al leads to $Fe_{50}Cr_{50}/Al_2O_3$ nanocomposites and Fe and Al_2O_3 to Fe/Al_2O_3 composites (7, 8).

A novel method for synthesizing metal–oxide composites is to use a disproportionation reaction leading to a metal on one side and to an oxide on the other side. This idea has been recently developed in our laboratory by using Fe(II) disproportionation in a liquid medium (9). It leads to an α-Fe/Fe_3O_4 composite made up of small grains of 0.5–1.5 μm in size which do not oxidize below 100°C in air. This is surprising since powders of magnetite or metal of such a fine granulometry oxidize rapidly at room temperature. This disproportionation reaction has also been used to synthesize other composites. Indeed, as metallic iron reduces Co(II) and Ni(II), it has been possible to obtain composites made up of iron–cobalt alloy (or iron–nickel alloy) and cobalt- (or nickel-) doped magnetite (9–14). The Co/Fe and Ni/Fe global ratios in the composite were equal to 0.5. The metal was crystallized in a bcc structure when cobalt was involved and in a fcc structure in the nickel case. The composition of the cobalt containing composite was determined by using Mössbauer spectroscopy, chemical analysis, and XRD measurements. The formula was $(Co_{0.8}Fe_{0.2})_{0.44}\ [Co_{0.62}Fe_{2.38}O_4]_{0.56}$ (13). By heating in vacuum, iron and cobalt distribution between the alloy and the spinel phase changes because of an exchange between both phases. This indicates that both phases are intimately mixed (11). The thermogravimetric analysis exhibited an oxidation above 250–300°C in air and a reversible transformation into a wüstite phase at 840°C in vacuum. However, the experimental conditions were not precisely determined. In this paper, we investigate the influence of various Co/Fe ratios on the composition of the composite. Two concentrations of potassium hydroxide are considered.

EXPERIMENTAL

The composites were synthesized according to the method described previously (10–12). Co(II) and Fe(II) chloride solutions in which the metal concentration is 2.5 mol/liter and with various Co/Fe ratios, $(Co/Fe)_i = 0$, 0.1, 0.33, 0.5, 0.66, 0.75, and 1, were added to either a 9.0 or a 11.5 mol/liter potassium hydroxide solution heated, respectively, at 120 or 130°C in a capped stainless steel vessel. The samples are, respectively, labeled 1 to 8 and 9 to 16. During the addition, the potassium hydroxide concentration decreased. However, the volumes of both solutions were chosen so that $[KOH]_f/[KOH]_i = 0.95$, i and f referring to the potassium hydroxide concentration before and after the addition of chlorides. Indeed, low quantities of material were synthesized, about 1.5–2 g. The precipitate was filtrated 20 min after the addition of chlorides. During the maturation time, the temperature of the solution in-

0022-4596/96 $18.00

creased up to 130°C when $[KOH]_i$ = 9.0 mol/liter and up to 140°C when $[KOH]_i$ = 11.5 mol/liter.

The characterization of the precipitate was performed by means of chemical analysis, XRD, TG, DTA, and magnetization measurements. The samples were chemically analyzed by the Laboratoire Central d'Analyse de Vernaison CNRS and the global $(Co/Fe)_f$ was determined. XRD data were collected at room temperature with a D500 Siemens diffractometer equipped with a primary beam quartz monochromator ($Co K\alpha_1$ = 1.78897 Å). TG and DTA measurements were carried out in platinum crucibles in air or in vacuum immediately after the synthesis by using a Setaram 92 apparatus. The heating rate was 2 K/min. The weight variation was calculated after removing the signal of the empty crucible. Magnetization was measured by using a FONER apparatus at room temperature.

RESULTS

1. XRD Characterization of the Crystallized Phases

The samples were first characterized by XRD measurements. All the samples exhibit well defined patterns with very low background. The patterns observed at room temperature for $(Co/Fe)_i$ = 0.1, 0.33, 0.66, 0.75 when $[KOH]_i$ = 9.0 mol/liter and for $(Co/Fe)_i$ = 0.66 when $[KOH]_i$ = 11.5 mol/liter are presented in Fig. 1.

In all the samples, a spinel phase and a metallic phase of the bcc structure isomorphous to α-Fe occur (Fig. 1). These phases have been already encountered in the composites previously described (9–12). The lattice constant of the spinel phase is always the same and is equal to 8.398 (2) Å. The unit cell parameter of the bcc phase varies due to $(Co/Fe)_i$ (Table 1). It decreases from 2.867(1) to 2.839 (1) Å for $[KOH]_i$ = 9.0 mol/liter and to 2.844 (2) Å for $[KOH]_i$ = 11.5 mol/liter when $(Co/Fe)_i$ increases. This decrease corresponds to a decrease of iron concentration in the alloy (15). Furthermore, with respect to those of the spinel phase, its diffraction lines are less intense when $(Co/Fe)_i$ = 0.66 or 0.75 and $[KOH]_i$ = 9.0 mol/liter. Let us note that the diffraction lines of the bcc phase of sample 2 ($(Co/Fe)_f$ = 0.090) are intense and broad. The width may result either from a distribution of composition, i.e., an heterogeneity of the metallic phase, or from a small grain size of the metallic phase.

Additional diffraction lines appear for $(Co/Fe)_i \geq 0.25$. Their interreticular distances are reported in Table 2. Their intensity increases when $(Co/Fe)_i$ increases and $[KOH]_i$ decreases (Fig. 1). Two indexations may be considered for these additional diffraction lines:

(i) The second and the third diffraction lines reported in Table 2 may correspond to a fcc structure isomorphous of cubic cobalt of which the lattice constant varies due to $(Co/Fe)_i$ (Table 1). It decreases when $(Co/Fe)_i$ increases. However, according to Pearson (15), the solid solution between cobalt and iron which would correspond to these lattice constants does not exist. The other diffraction lines are close to the four most intensive diffraction lines of hexagonal cobalt, but unhappily they cannot be indexed according to this structure.

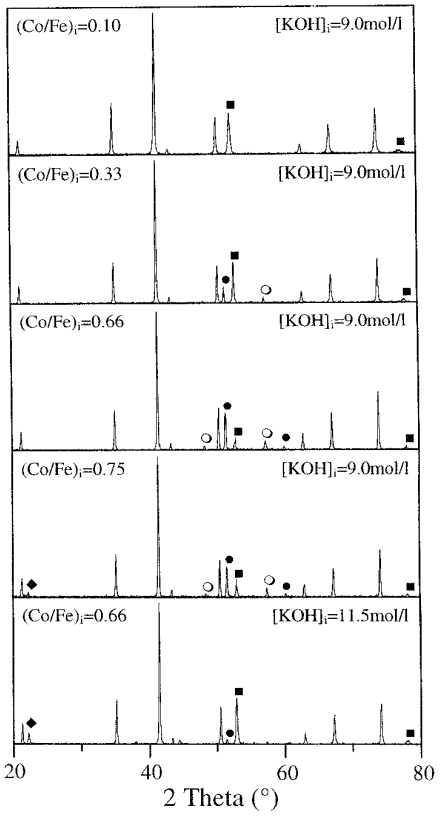

FIG. 1. XRD patterns recorded at room temperature for $(Co/Fe)_i$ = 0.1, 0.33, 0.66, 0.75 when $[KOH]_i$ = 9.0 mol/liter and for $(Co/Fe)_i$ = 0.66 when $[KOH]_i$ = 11.5 mol/liter. ■ and ◆ refer to bcc and β-$Co(OH)_2$, respectively, and ● and ❍ to the additional diffraction lines, ● corresponding to the diffraction lines that can be indexed in a fcc structure. The other diffraction lines are those of the spinel phase.

(ii) All the additional diffraction lines may be indexed in a hexagonal system with a = 7.136(2) Å and c = 2.186(2) Å. a is thus the double of the cubic parameter of fcc structure. However, that would mean that this metallic structure is not dense which is very unlikely for a metal.

The additional diffraction lines are less intense when $[KOH]_i$ = 11.5 mol/liter, i.e., when the temperature of KOH is higher than 130°C (Fig. 1). Furthermore, they disappear when the composites are heated above 170°C. At the same time, the diffraction lines of the bcc phase strongly increase. That means that the phases corresponding to the additional diffraction lines transform into the metallic bcc phase, and so are metallic. The reverse transformation (appearance of the additional diffraction lines with decreasing bcc diffraction lines) is never observed, showing that they have a limited stability.

TABLE 1
Co/Fe Ratios in the Initial Chloride Solution ($(Co/Fe)_i$) and in the Composite ($(Co/Fe)_f$), Lattice Parameters of bcc and fcc-Metallic Phases, and Composition of bcc Metallic Phase Deduced from W.B. Pearson (15)

Sample	$[KOH]_i$ (mol/liter)	β-$Co(OH)_2$	$(Co/Fe)_i$	$(Co/Fe)_f$	a_{bcc} (Å)	% Fe in the bcc structure	a_{fcc} (Å)
1	9.0		0	0	2.867(1)	100	
2	9.0		0.1	0.090(2)	2.864(1)	69(1)	
3	9.0		0.25	0.21(1)	2.850(1)	40(1)	3.584(5)
4	9.0		0.33	0.27(1)	2.845(1)	33(1)	3.574(2)
5	9.0		0.50	0.37(1)	2.841(1)	26(1)	3.570(2)
6	9.0		0.66	0.41(1)	2.841(1)	26(1)	3.571(2)
7	9.0	yes	0.75		2.839(1)	15(1)	3.569(2)
8	9.0	yes	1		2.839(1)	15(1)	3.565(2)
9	11.5		0	0	2.866(1)	100	
10	11.5		0.1	0.095(2)	2.863(1)	67(1)	
11	11.5		0.25	0.20(1)	2.852(1)	43(1)	3.587(5)
12	11.5		0.33	0.23(1)	2.848(1)	38(1)	3.580(3)
13	11.5		0.50	0.34(1)	2.846(1)	34(1)	3.577(3)
14	11.5	yes	0.66		2.846(1)	34(1)	3.577(2)
15	11.5	yes	0.75		2.844(1)	32(1)	3.574(2)
16	11.5	yes	1		2.844(1)	32(1)	3.574(2)

When $(Co/Fe)_i \geq 0.75$ for $[KOH]_i = 9.0$ mol/liter and 0.66 for $[KOH]_i = 11.5$ mol/liter, β-$Co(OH)_2$ is detected by XRD measurements, so that the composite cannot be considered pure. The quantity of β-$Co(OH)_2$ increases with a further increase in cobalt concentration. As these samples are not pure, they are not studied in the following.

2. Chemical Analysis

The Co/Fe global ratios in the samples, $(Co/Fe)_f$, are reported in Table 1 for the samples that do not contain cobalt hydroxide. One can note that $(Co/Fe)_f < (Co/Fe)_i$ which means that cobalt hydroxide dissolves in the potassium hydroxide solution and is lost in the filtrate. The difference is higher for high $(Co/Fe)_i$ and for the most concentrated KOH solution. When important quantities of cobalt hydroxide are dissolved, it precipitates again during the filtration, and is then detected by XRD measurements.

3. TG and DTA in Air and in Vacuum

In vacuum, no weight variation occurs. DTA curves exhibit one endothermic peak (Fig. 2). For $(Co/Fe)_f = 0$, the transition occurs at 570°C (9). This corresponds to the reaction between Fe and Fe_3O_4 which transforms into the wüstite phase $Fe_{1-x}O$. This reaction was described several decades ago (16–20). When cobalt is added in low quantities, for instance for $(Co/Fe)_i = 0.1$, a large peak is observed between 680 and 900°C in the DTA curve. When $(Co/Fe)_f$ increases, the peak becomes thinner and is moved toward higher temperatures, 880°C for $(Co/Fe)_f = 0.41$. Thus, on one side, cobalt increases the transition temperature, and on the other side, the broadness of peaks means that some zones are richer in cobalt than others. This is particularly visible when $(Co/Fe)_f = 0.090$. One can conclude that the homogeneity of both phases of the composite, the metal on one side and the spinel on the other side, is improved when the Co/Fe ratio increases. The weight variation in air is similar to that previously observed; i.e., a strong weight increase characteristic to an oxidation occurs (12). The temperature at which the strong weight increase occurs T_{ox} and the weight increase $\Delta m/m$ are reported in Table 3. No correlations between T_{ox} on the one hand and $(Co/Fe)_i$ and $[KOH]_i$ on the other hand have been encountered. $\Delta m/m$ varies due to the $(Co/Fe)_i$ ratio. It characterizes the capacity of the composite to be oxidized into a mixture of Fe(III) and Co(II) oxides. As Co(II) is introduced at the beginning, $\Delta m/m$ corresponds at maximum to the oxidation of Fe(II) of the initial solution. So $\Delta m/m$ decreases when $(Co/Fe)_f$ increases in the composite. By using $\Delta m/m$ values and $(Co/Fe)_f$ determined by chemical analysis, and assuming that the different alloys have the composition of the bcc phase, we have determined the chemical formulas. They are reported in Table 3. Let us note that the metal is present in highest quantities for the highest $[KOH]_i$.

After the composites have spent several months in air, a weight decrease is observed in vacuum between 20 and 400°C, particularly for $(Co/Fe)_i = 0.5$ and 0.66. It indicates that hydrates and carbonates have been formed on the surface. Thus, these samples must be kept in a controlled

TABLE 2
Interreticular Distances d_{hkl} and Intensities I of Additional Diffraction Lines When $[KOH]_i$ = 9.0 mol/liter Compared with Those of Cubic and Hexagonal Cobalt

	Additional diffraction lines											
Sample	d_{hkl} (Å)	I	d_{hkl} (Å)	I	d_{hkl} (Å)	I	d_{hkl} (Å)	I	d_{hkl} (Å)	I	d_{hkl} (Å)	I
3			2.069(2)	7	1.872(1)	3.5	1.792(2)	2				
4			2.063(2)	12	1.867(1)	4.3	1.787(2)	1			1.192(1)	1.6
5	2.186(1)	2.7	2.061(2)	27	1.864(1)	6.7	1.785(2)	3	1.237(1)	1.7	1.190(1)	3.8
6	2.186(1)	3	2.061(2)	27	1.865(1)	6.5	1.788(2)	3	1.236(1)	2.7	1.190(1)	5
7	2.185(1)	2.4	2.060(2)	22	1.863(1)	7	1.785(2)	3	1.236(1)	1	1.189(1)	2.7
8	2.184(1)	1.7	2.058(2)	19	1.863(1)	5.2	1.783(2)	2			1.189(1)	3.5
Co*Fm3m* JCPDS 15-806			2.0467	100			1.7723	40				
Co$P6_3/mmc$ JCPDS 5-727	2.165	20			1.910	100			1.252	80	1.149	80

Note. The intensity of the most intense diffraction line of the spinel phase is 100.

atmosphere in contrast to the composites previously synthesized (10–12).

4. Saturation Magnetization and Coercive Field at Room Temperature

The variations of saturation magnetization σ_s and coercive field H_c are given in Fig. 3 when $[KOH]_i$ = 9.0 mol/liter. The increasing $(Co/Fe)_f$ in the composite results in an increase in coercive field. Let us note that the extrapolation of coercive field for $(Co/Fe)_f$ = 0.50 leads to 1200 Oe, a value lower than that measured in previous work for this composition which was 2300 Oe (10). Saturation magnetization seems to decrease when $(Co/Fe)_f$ increases. The same range of values is found for $[KOH]_i$ = 11.5 mol/liter.

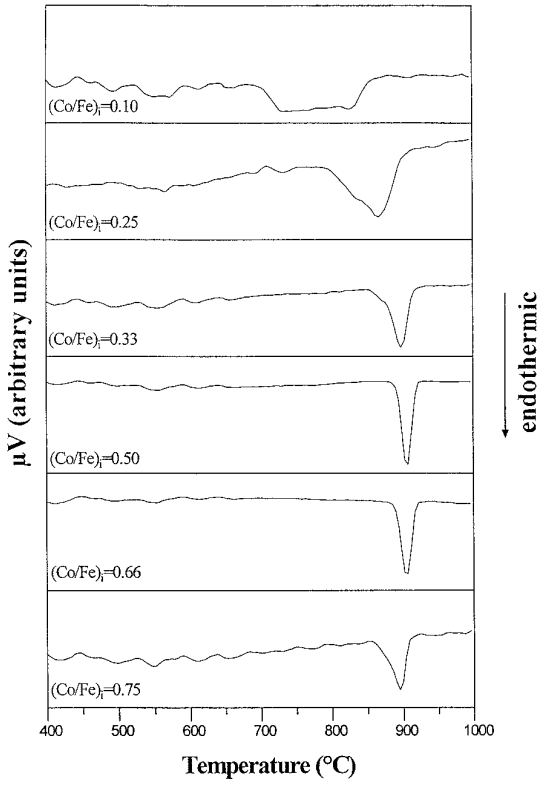

FIG. 2. DTA curves recorded in vacuum for $(Co/Fe)_i$ = 0.1, 0.25, 0.33, 0.5, 0.66, 0.75, and $[KOH]_i$ = 9.0 mol/liter.

DISCUSSION AND CONCLUSION

Metal–spinel composites made up of iron–cobalt alloy and cobalt doped magnetite have been obtained by disproportionation and dehydration of $Fe(OH)_2$ and reduction of Co(II) by Fe^0, in hot and concentrated KOH solution,

TABLE 3
Temperatures above Which an Oxidation Occurs (T_{ox}), Weight Variations ($\Delta m/m$) by TG in Air up to 1000°C, and Chemical Formula Deduced from TG Measurements, the Chemical Analysis, and Assuming That All the Metallic Phases Have the Composition of the bcc Phase

Sample	T_{ox} (°C)	$\Delta m/m$ (%)	Chemical formula
1	110	8.5	$Fe^0_{0.39}[Fe_3O_4]_{0.61}$
2	100	8.6	$(Co^0_{0.31}Fe^0_{0.69})_{0.43}[Co_{0.08}Fe_{2.92}O_4]_{0.57}$
3	213	8.0	$(Co^0_{0.60}Fe^0_{0.40})_{0.45}[Co_{0.17}Fe_{2.83}O_4]_{0.55}$
4	231	7.4	$(Co^0_{0.67}Fe^0_{0.33})_{0.44}[Co_{0.28}Fe_{2.72}O_4]_{0.56}$
5	214	7.7	$(Co^0_{0.74}Fe^0_{0.26})_{0.49}[Co_{0.37}Fe_{2.63}O_4]_{0.51}$
6	251	6.5	$(Co^0_{0.74}Fe^0_{0.26})_{0.44}[Co_{0.52}Fe_{2.48}O_4]_{0.54}$
9	182	9.5	$Fe^0_{0.43}[Fe_3O_4]_{0.57}$
10	100	8.7	$(Co^0_{0.33}Fe^0_{0.67})_{0.44}[Co_{0.07}Fe_{2.93}O_4]_{0.56}$
11	280	8.4	$(Co^0_{0.57}Fe^0_{0.43})_{0.47}[Co_{0.15}Fe_{2.85}O_4]_{0.53}$
12	208	8.2	$(Co^0_{0.62}Fe^0_{0.38})_{0.47}[Co_{0.52}Fe_{2.48}O_4]_{0.53}$
13	228	8.1	$(Co^0_{0.66}Fe^0_{0.34})_{0.49}[Co_{0.36}Fe_{2.64}O_4]_{0.51}$

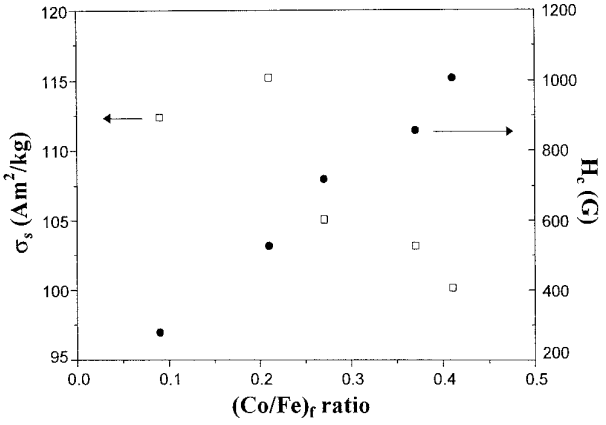

FIG. 3. Variation of saturation magnetization σ_s and coercive field H_c at room temperature versus $(Co/Fe)_f$ for $[KOH]_i$ = 9.0 mol/liter.

for Co/Fe ratios of the initial chloride solution between 0 and 1. The evaporation has been limited, and the volumes of KOH and chlorides have been chosen so that the concentration of potassium hydroxide is nearly constant during the reaction. Furthermore, the temperature during the precipitation and maturation time has only increased by 10°C.

The following facts emerge from these studies:

• The disproportionation of $Fe(OH)_2$ occurs for all the ratios Co/Fe between 0 and 1. Metallic and spinel phases are always detected by XRD measurements.

• The spinel phase is a solid solution between magnetite and cobalt ferrite. As both phases have very close lattice constants, $a(Fe_3O_4)$ = 8.396 Å and $a(CoFe_2O_4)$ = 8.392 Å, the variation of composition of the spinel phase due to $(Co/Fe)_i$ and $(Co/Fe)_f$ could not be pointed out.

• The metallic phases present several structures whose respective concentrations depend on $(Co/Fe)_i$ and $[KOH]_i$ values: the bcc structure is more important for low $(Co/Fe)_i$ and high $[KOH]_i$, while the other metallic phases are favored by high $(Co/Fe)_i$ and low $[KOH]_i$. The structures of the latter are not clear, but as they are metastable (they disappear by heating above 170°C and do not crystallize again by cooling), it would not be surprising that they correspond to particular metallic structures, which have not been encountered yet.

• The important parameter for the crystallization of the metal in the bcc structure is probably the temperature. Indeed, on the one side, the additional diffraction lines disappear when the composites are heated above 170°C and, on the other side, they are not observed when the rate of disproportionation is high, i.e., for the highest concentrations of Fe(II) and KOH. Indeed, the disproportionation of Fe(II) being highly exothermic, it would not be surprising that, in this latter case, the surface temperature of particles reaches 170–200°C although the solution is at 130°C.

• The variation of Co/Fe ratio allows one to prepare composites with various composition, the increasing Co/Fe values resulting in an increase of cobalt concentration in both phases.

• Cobalt hydroxide dissolves in high concentrated KOH. This results in (i) a $(Co/Fe)_f$ ratio lower in the composite than in the initial solution; (ii) a recrystallization of cobalt hydroxide during the filtration for high cobalt concentration in the filtrate, because the temperature and the basicity decrease.

• The phases involved in the composites with low concentration of cobalt are heterogeneous in agreement with the broadness of the XRD lines and the wide temperature range for the transition to the wüstite structure.

In contrast to previous works, this study points out the dissolution of cobalt hydroxide in KOH and the crystallization of metallic phases different from bcc iron–cobalt alloy. In addition, these composites are not well protected toward the oxidation and hydration of air. However, in previous works, the basicity of the medium and the temperature were not controlled. The basicity decreased during the addition of the chloride solution. Consequently, cobalt was not lost in the filtrate. By evaporation, the concentration of potassium hydroxide increased during the maturation time and also its temperature increased. So, the metallic phase was of bcc structure and, in addition, the external layer, which protected the grain, was probably more crystallized and more resistant.

In conclusion, the concentration of potassium hydroxide and its variation during the precipitation appear to be very important for the physical properties. It would be of interest to precisely determine the relation between the processing and the microstructure of the grains by using, for instance, transmission electron microscopy. These studies are in progress.

REFERENCES

1. R. E. Newnham and S. Trolier-McKinstry, *J. Appl. Crystallogr.* **23,** 447 (1990).
2. J. J. Mecholsky, Am. Ceram. Soc. Bull. **65,** 315 (1986).
3. H. Tamagawa, K. Oyama, T. Yamaguchi, H. Tanaka, H. Tsuiki, and A. Ueno, *J. Chem. Soc. Faraday Trans.* **83,** 3189 (1987).
4. C. Estournes, N. Cornu, and J. L. Guille, *J. Non Cryst. Solids* **170,** 287 (1994).
5. A. Marchand, B. Barbara, P. Mollard, G. Fillion, X. Devaux, and A. Rousset, *J. Magn. Magn. Mater.* **116,** 64 (1992).
6. Ch. Laurent, J. J. Demai, A. Rousset, K. R. Kannan, and C.N.R. Rao, *J. Mater. Res.* **9,** 229 (1994).
7. T. Ambrose, A. Gavrin, and C. L. Chien, *J. Magn. Magn. Mater.* **116,** L311 (1992).
8. P. Matteazi and G. Le Caer, *J. Am. Ceram. Soc.* **75,** 2749 (1992).
9. S. Läkamp, A. Malats i Riera, G. Pourroy, P. Poix, J. L. Dormann, and J. M. Greneche, *Eur. J. Solid State Inorg. Chem.* **32,** 159 (1995).

10. A. Malats i Riera, G. Pourroy, and P. Poix, *J. Magn. Magn. Mater.* **125,** 125 (1993).
11. A. Malats i Riera, G. Pourroy, and P. Poix, *J. Alloys Compounds* **202,** 113 (1993).
12. A. Malats i Riera, G. Pourroy, and P. Poix, *J. Solid State Chem.* **108,** 362 (1994).
13. J. L. Dormann, A. Malats i Riera, G. Pourroy, P. Poix, J. Jove, and P. Renaudin, *Hyperfine Interactions* **94,** 1995 (1994).
14. G. Pourroy, S. Ferlay, and J. L. Dormann, *Eur. J. Solid State Inorg. Chem.* **32,** 313 (1995).
15. W. B. Pearson, ''Handbook of Lattice Spacings and Structures of Metals'' p. 505. Pergamon, Elmsford, NY, 1964.
16. G. Chaudron, *C. R. Acad. Sci.* **172,** 152 (1921).
17. G. Chaudron, and H. Forestier, *C. R. Acad. Sci.* **178,** 2173 (1924).
18. R. Collongues and G. Chaudron, *C. R. Acad. Sci.* **234,** 728 (1952).
19. B. Ilschner and E. Mlitzke, *Acta Metall.* **13,** 855 (1965).
20. N. N. Greenwood and A. T. Howe, *J. Chem. Soc. Dalton Trans.* **1,** 110 (1972).